

RBP-DIP: High-Quality CT Reconstruction Using an Untrained Neural Network with Residual Back Projection and Deep Image Prior

Ziyu Shu, Alireza Entezari

Abstract—Neural network related methods, due to their unprecedented success in image processing, have emerged as a new set of tools in CT reconstruction with the potential to change the field. However, the lack of high-quality training data and theoretical guarantees, together with increasingly complicated network structures, make its implementation impractical. In this paper, we present a new framework (RBP-DIP) based on Deep Image Prior (DIP) and a special residual back projection (RBP) connection to tackle these challenges. Comparing to other pre-trained neural network related algorithms, the proposed framework is closer to an iterative reconstruction (IR) algorithm as it requires no training data or training process. In that case, the proposed framework can be altered (e.g, different hyperparameters and constraints) on demand, adapting to different conditions (e.g, different imaged objects, imaging instruments, and noise levels) without retraining. Experiments show that the proposed framework has significant improvements over other state-of-the-art conventional methods, as well as pre-trained and untrained models with similar network structures, especially under sparse-view, limited-angle, and low-dose conditions.

Index Terms—Limited-angle CT reconstruction, sparse-view CT reconstruction, deep image prior, untrained neural network.

I. INTRODUCTION

NEURAL network related algorithms have provided a new paradigm in Computed tomography (CT) reconstruction that may change the field. Reconstruction methods in this area are designed to learn the best way of reconstruction by training with previous data. In addition to building end-to-end reconstruction algorithms [1], [2], neural networks can also work as plugins, enhancing the performance of any procedures in conventional reconstruction methods [3]–[5]. Although promising results have been observed, neural network related algorithms face their own challenges:

First, neural network related algorithms are brittle because they do not follow common human perception. Instead of learning the correct transformation between input (sinogram signals) and output (reconstructed images), neural network related algorithms only learn a correlation without understanding

the causation. A neural network related algorithm may be able to reconstruct a lung CT image perfectly, but it doesn't mean that the algorithm perceives the mathematical relationship between X-ray projections and the reconstructed image or the structure of the patient's lung. In fact, it only indicates that based on the previous training data, the current output and input tend to match statistically. Also, such statistics can be easily broken as the circumstances change. It is possible for neural networks to ignore small abnormal changes that are seen as symbols of illness by radiologists, and cause severe consequences [6]. Hence, using neural network related algorithms in medical image reconstruction risks missing patient-specific features.

Secondly, pre-trained models are trained to minimize an objective function (loss function) on only the training data but not the inference data. There is no guarantee that the output of an inference input will also have a minimum loss. Thus, large-scale well-annotated datasets are crucial for obtaining accurate and versatile models. For example, one of the most widely used image datasets, ImageNet [7], contains more than 1.2 million categorized natural images of 1000+ classes. Neural network models trained on this dataset achieved extraordinary results. However, there is no comparable large-scale medical image datasets. CT reconstruction benchmarks such as the LIDC-IDRI [8] (Lung Image Database Consortium Image Collection) dataset only contains 1018 patients, which is insufficient to properly train a deep neural network for patients of all demographics. This is mainly due to the difficulty of data acquisition and annotation. In practice, ground truth is mostly obtained with high-dose reconstructions, which implies that patients have to be exposed to high doses of X-ray radiation. Also, quality annotation can only be done by professional radiologists.

Furthermore, without considering the inference data, neural network related algorithms cannot even generate optimal results for training inputs. The loss function of a neural network is minimized for all training data on average during the training process. This implies that such minimization may not work for every single training instance. For example, given a neural network whose losses on training instances A and B are 0 and 10 (in that case, the neural network is optimized for A but not for B, and the average loss is 5), the current training algorithms tend to update the neural network to change the losses to 3 for both, where both the training instances are

Manuscript submitted September 9, 2022. This work was supported in part by the NSF [grant number CCF-2210866]

Ziyu Shu and Alireza Entezari are with the CISE department, University of Florida 32603, USA (email: ziyushu@ufl.edu; entezari@ufl.edu).

unoptimized for, but the average loss is smaller than before. Even if the average loss is minimized to 0 for every training data, such a model may be considered impractical due to the suspicion of overfitting. In fact, multiple techniques such as regularization and early stopping are implemented to avoid the complete minimization of the loss function.

Last but not least, neural network related algorithms are costly. On the one hand, training neural network algorithms are time-consuming. A single neural network can only handle inference input with the same distribution as the training data. A network has to be retrained for every specific setting (e.g. reconstruction resolution, sinogram domain sampling ratio, noise level, imaging objects, etc.) to achieve the highest performance. Hence, we need hundreds of different networks to handle that many different settings in practice. On the other hand, analyzing and improving a given neural network is also resource intensive. There is no systematic and efficient way to improve the performance of a neural network if it doesn't meet expectations. In practice, our options are limited. We can either improve the quality of training data (acquiring more data, data argumentation) or change the structure of the given neural network using rules of thumb. It is evident that neither method is efficient due to the lack of clear theoretical guidance.

All the aforementioned challenges make the neural network related CT reconstruction algorithms unstable. As a result, these algorithms are mostly considered impractical, since medical imaging requires reliable and trustworthy methods.

In this paper, a new framework (RBP-DIP) for CT reconstruction is proposed. An untrained U-net with a newly proposed RBP (residual back projection) connection is used for reconstruction: its weights are optimized to match the observed measurements, and its input is updated iteratively by the conventional iterative reconstruction (IR) algorithm during the reconstruction process. In fact, the proposed framework can be regarded as an IR method that uses a randomly initialized neural network and gradient descent rule but not conventional linear optimization algorithms to minimize the objective function (loss function). The proposed framework has no training process and does not require a training dataset. Thus, the problems caused by the training process can be mitigated. The extraordinary abilities of neural networks guarantee that the difference between the measurement and reconstruction results can be minimized. The DIP and the newly designed RBP connection help the model generate more reasonable and detailed results. The experiments show that the proposed framework provides significant improvements over conventional methods and neural network models (both untrained and pre-trained) with a similar network structure, especially under sparse-view, limited-angle, and low-dose conditions.

The remainder of this paper is organized as follows: the details of the CT reconstruction problem and the related works are introduced in Section II. The proposed framework is introduced in Section III, it is compared with conventional methods, pre-trained and untrained methods with the similar network structure on real CT images under different conditions in Section IV. The corresponding discussion is in Section V. The conclusion of this study is presented in Section VI.

II. RELATED WORKS

A. Computed Tomography and Model Based Iterative Reconstruction

CT is a critical technology with a wide range of applications in biomedical imaging. The well-known filtered back projection (FBP) algorithm is computationally efficient but requires a large number of high-quality views. This is because it is derived from the analytic inversion of the Radon transform and does not account for any non-ideal effects. To solve this problem, model based iterative reconstruction (MBIR) is proposed. It integrates models of X-ray physics, non-ideal effects, and image priors into the reconstruction algorithm. The forward model of MBIR can be expressed as a matrix:

$$\mathbf{g} = \mathbf{A}\mathbf{c} = \begin{bmatrix} \mathcal{P}_{\theta_1}(\psi_1) & \cdots & \mathcal{P}_{\theta_1}(\psi_n) \\ \vdots & & \vdots \\ \mathcal{P}_{\theta_m}(\psi_1) & \cdots & \mathcal{P}_{\theta_m}(\psi_n) \end{bmatrix} \begin{bmatrix} c_1 \\ \vdots \\ c_n \end{bmatrix}, \quad (1)$$

where \mathcal{P}_{θ} indicates the forward operator at projection angle θ . \mathcal{P}_{θ} can be Radon transform for 2D parallel-beam CT reconstruction under ideal conditions, or other transforms for more complex cases [9]–[12]. θ_1 to θ_m indicate m projection angles, ψ_1 to ψ_n indicate a discretization kernel (e.g. pixel for 2D and voxel for 3D) at different locations, c_1 to c_n indicate corresponding coefficients representing the attenuation map of an imaged object:

$$f_{\psi} = \sum_{i=1}^n c_i \psi_i, \quad (2)$$

MBIR obtains the reconstruction result by minimizing the inconsistency between the measurement and the reconstruction result ($\|\mathbf{g} - \mathbf{A}\mathbf{c}\|^2$). Such minimization can be achieved by iteratively back projecting the current residual to the image domain ($\mathbf{A}^T(\mathbf{g} - \mathbf{A}\mathbf{c}) = \mathbf{A}^T\mathbf{g} - \mathbf{A}^T\mathbf{A}\mathbf{c}$). High-quality reconstruction results can be obtained under non-ideal conditions once an accurate forward model is available [9], [13].

However, MBIR has its own deficiencies. According to the central slice theorem (Fourier slice theorem), back projections at certain projection angles can update only the corresponding frequency slices in the frequency domain. Examples are shown in Fig.1. Due to the missing projections, the sparse-view CT reconstruction in the frequency domain is non-zero only at specific angles (Fig.1b), and the limited-angle CT reconstruction in the frequency domain is missing its second and fourth quadrants (Fig.1c). As a result, the high-quality sparse-measurement (sparse-view or limited-angle) CT reconstruction cannot be directly obtained by MBIR as some of the projection views are missing. To solve this problem, researchers proposed utilizing the sparsity of the imaged object to improve the reconstruction quality, resulting in the following unconstrained optimization problem:

$$\arg \min_{\mathbf{c}} \|\mathbf{g} - \mathbf{A}\mathbf{c}\|^2 + \lambda R(\mathbf{c}), \quad (3)$$

where R indicates constraints. Researchers proposed multiple constraints for different conditions. The total variation constraint [14] utilizes the piece-wise constant prior of the reconstruction results to remove the noise and artifacts. Jin et al. [15] proposed using the anisotropic total variation to better handle

the directional artifacts caused by limited-angle CT reconstruction. Reweighted anisotropic total variation [16] approximates the l_0 -norm instead of using l_1 -norm. Anisotropic relative total variation [17] uses the windowed inherent variation and the windowed total variation to better utilize images' structural information. The Markov random field related methods [18]–[20] proposed using a potential function to utilize the piecewise constant prior while better preserving sharp edges. As a result, MBIR with constraints uses the forward and back projection scenario to update the frequency pixels in the measured area and uses the aforementioned constraints to inpaint the unknown area. However, its performance is still limited by incomplete projections, especially when the number or the angular range of the projections is too small. To overcome this challenge, multiple neural network related methods are proposed.

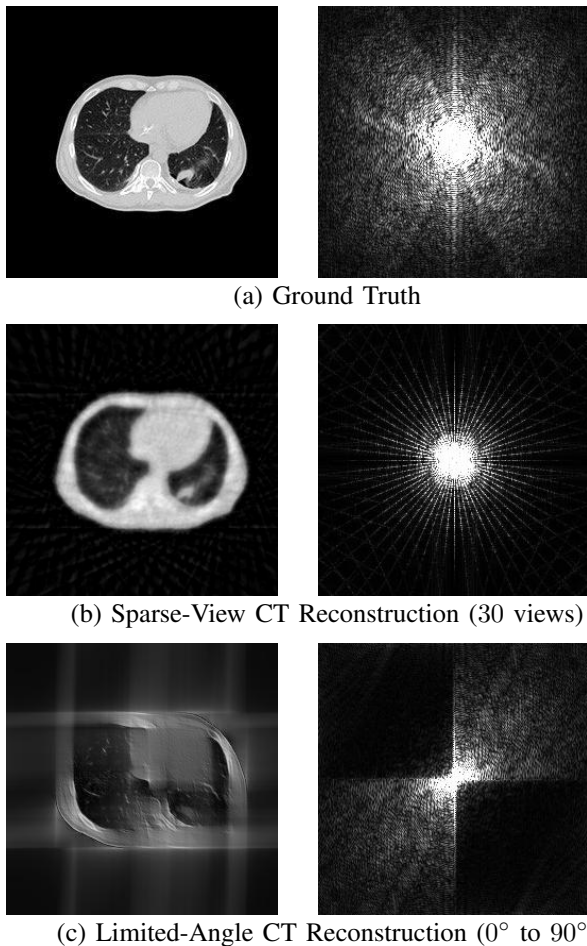


Fig. 1: MBIR can update only the measured frequency slices. (a) Ground truth in the image and frequency domain; (b) sparse-view CT reconstruction in the image and frequency domain; (c) limited-angle CT reconstruction in the image and frequency domain.

B. Neural Network Related Methods

Neural networks can be used for CT reconstructions. Zhu et al. [1] proposed a unified, end-to-end reconstruction frame-

work called AUTOMAP to do CT reconstructions. The model consists of two convolutional layers and three large fully connected layers. The analysis of its activation values as well as convolutional kernels at different layers demonstrates that AUTOMAP acts like a compressed sensing algorithm and can generate high-quality reconstructions. Also, its impressive performance reveals the great potential of neural network related methods in the medical imaging area. In the past several years, more research was made to improve its performance and overcome the challenges described in Section I.

Instead of using an end-to-end reconstruction algorithm to learn a direct transformation from sinogram to reconstruction result, researchers tried to inject more information into the input to simplify the task of neural networks. Zhang et al. [21], Chen et al. [5], and Ye et al. [22] proposed using back projections, filtered back projections, and single-view back projections as the input respectively. In that case, neural networks only need to focus on the transformations which are non-analytical (e.g. noise and artifacts removal) instead of analytical transformations such as the Radon transform. Another potential method is using a neural network to represent these analytical transformations, which is available from [23]. Recently, more delicate models were proposed, where multiple neural networks focusing on different tasks collaborate for better performance. Yin et al. [24] proposed using two neural networks to denoise both the sinogram domain and image domain. Hu et al. [25] and Zhang et al. [26] proposed using three neural networks. In addition to the two denoising neural networks in [24], an extra image domain discriminator for the real and reconstructed images is introduced to further guide the model. To utilize that many sub-networks, increasingly complicated multi-loss functions are proposed. For example, the multi-loss function in [26] contains five losses, four comparing the differences between the denoised sinogram, FBP of the denoised sinogram, reconstructed image, sinogram of the reconstructed image and their corresponding ground truth, with the last one being the loss function for the discriminator. As mentioned in Section I, these methods are not suitable for large-scale implementation. The cascade of multiple sub-networks makes the problem even worse, as the errors may be amplified level by level and cannot be diagnosed easily. Furthermore, the complex structures of these models are unsuitable for efficient training. As a result, these models always lack versatility and have to be trained for each specific scenario (different sampling rate, noise level, etc.) at a very high cost.

Multiple techniques are proposed to overcome the limitation caused by the lack of training data. Some researchers proposed using the transfer learning technique, as they believe that pre-training on other datasets such as ImageNet can help the neural network to better extract meaningful features [27]–[29]. However, the differences between CT images and natural images (e.g. streak artifacts, which do not exist in natural images) cannot be ignored. Some researchers proposed using the data augmentation technique, where the amount of data can be greatly increased by adding slightly modified copies of already existing data or new synthetic data created from existing data. However, the current argumentation methods

(affine transform, cropping, adding Gaussian or Poisson noise) may be unable to well model the practical differences caused by the uniqueness of patients and other non-ideal factors. Another potential method is patch-based learning [5], where multiple small patches can be extracted from a single image. Although the method obtained impressive results in the image denoising area, it may be unable to handle the CT reconstruction problem, as the rule of transformation cannot be learned from each individual patch.

The inverse generative adversarial network (inverse GAN) [30] methods can also partially solve the problem, where the latent vector z of a pre-trained generator $G(z; w)$ is optimized by solving the problem:

$$z^* = \arg \min_z \|g - AG(z; w)\|_2^2, \hat{c} = G(z^*; w), \quad (4)$$

this guarantees that at least a local minimum of the objective function can be found in the space spanned by the generator G . However, to obtain a high-quality result, an appropriate pre-trained model is still necessary.

In order to be free from the dependency on training data, some researchers proposed methods that require less or even no training data. For example, Zhang et al. [31] proposed a super-resolution method that generates high-resolution output from input by learning the relationship between the down-sampled input and the original input. However, the idea cannot be implemented in sparse-measurement and low-dose CT reconstruction, as the input images may contain incorrect information, such as artifacts and noise.

Ulyanov et al. [32] pointed out that the structure of a convolutional network itself is sufficient to capture plenty of low-level image statistical prior and thus can generate high-quality images in standard inverse problems. This property is called deep image prior (DIP). Implementations on CT reconstruction are available from [33]–[35]. Instead of using a pre-trained neural network, researchers proposed using untrained networks such as a generator or a U-net and optimizing their weights directly during the reconstruction process. The inputs of the networks are randomly initialized and then fixed [33], [34], which can be expressed as:

$$w^* = \arg \min_w \|g - AG(w; z)\|_2^2, \hat{c} = G(w^*; z), \quad (5)$$

where \hat{c} indicates the coefficients that we are trying to get, A indicates the measurement matrix, and $G(w; z)$ represents a convolutional neural network. The neural network takes z as the input and is parameterized by the weights w . This method was further improved by Shu et al. [35], where the latent vector will also be updated together with the weights to enhance the neural network's capability, and the normal operator of matrix A is used to greatly accelerate the calculation of iteration:

$$w^*, z^* = \arg \min_{w, z} \|A^T g - A^T AG(w, z)\|_2^2, \hat{c} = G(w^*, z^*). \quad (6)$$

Currently, these methods are far from mature, as they are not stable enough and cannot generate detailed images. As a result, Venn et al. [33] proposed running the same algorithm multiple times and choosing the best result; Bagger et al. [34] proposed introducing extra pre-trained neural networks for pre-

and post-processing. However, the former relies on inefficient trial and error, and the latter introduces pre-trained models again, which acts against its original purpose. The improved method proposed by [35] cannot fully solve these problems. Although high-quality reconstruction results can be obtained under sparse-measurement conditions, there is no substantial improvement in reconstruction results as the number and angular range of views increase.

III. PROPOSED METHOD

In each of its reconstruction iterations, MBIR related methods update the result by back projecting the residual between the current result and the measurement. They have the theoretical guarantee of perfect reconstruction when the number of views is enough, but will generate artifacts under the sparse-measurement condition (Fig.1a, Fig.1b, Fig.2b, and Fig.3b). On the other hand, the DIP related methods force an untrained neural network to optimize its weights to minimize the aforementioned residual. The DIP guarantees that a reasonable result will be obtained with high probability even under the sparse-measurement condition. However, DIP related methods suffer from blurring and neural network specific artifacts which may mislead radiologists (Fig.2d and Fig.3d). Our proposed method (RBP-DIP) can obtain a better result (Fig.2c and Fig.3c) by utilizing the advantages of both aforementioned methods. The architecture of the proposed method is shown in Fig.4.

The main architecture of the proposed method is the U-net, which has been proven effective in multiple image processing problems. The skip connection indicates that the network actually learns the difference between the input and output. It is worth mentioning that the skip connection is unnecessary for regular DIP related methods since their input is initialized randomly. However, for our RBP-DIP model, the skip connection is meaningful since the input of our model will be updated by the RBP connection. In fact, the RBP connection is the key difference between our RBP-DIP model and the DIP model in [33], [35]. In each reconstruction iteration, the input of our model will be updated by the residual between the current network output and the given measurement (sinogram signal in our case) using a conventional MBIR updating algorithm through the RBP connection. Note that the RBP connection is not involved in backpropagation.

The reconstruction process of RBP-DIP is shown in Algorithm.1, where lines 1, 3, 4, and 6 correspond to the steepest descent algorithm and can be replaced by any other MBIR algorithms. Lines 5 and 7 correspond to neural network optimization. In our proposed method, $z = c + \alpha\beta r$, the output c corrected by the RBP connection $\alpha\beta r$, can affect the next iteration's output directly by the skip connection and indirectly by $G(w; z)$ (line 5). We believe that the iteratively corrected z can better guide the model, as the correction mostly focuses on the edges and neural network specific artifacts.

In the Algorithm.1, β can be expressed as:

$$\beta = \frac{10^{-3}}{1 + e^{-\left(\frac{n}{n_s} - n_c\right)}}, \quad (7)$$

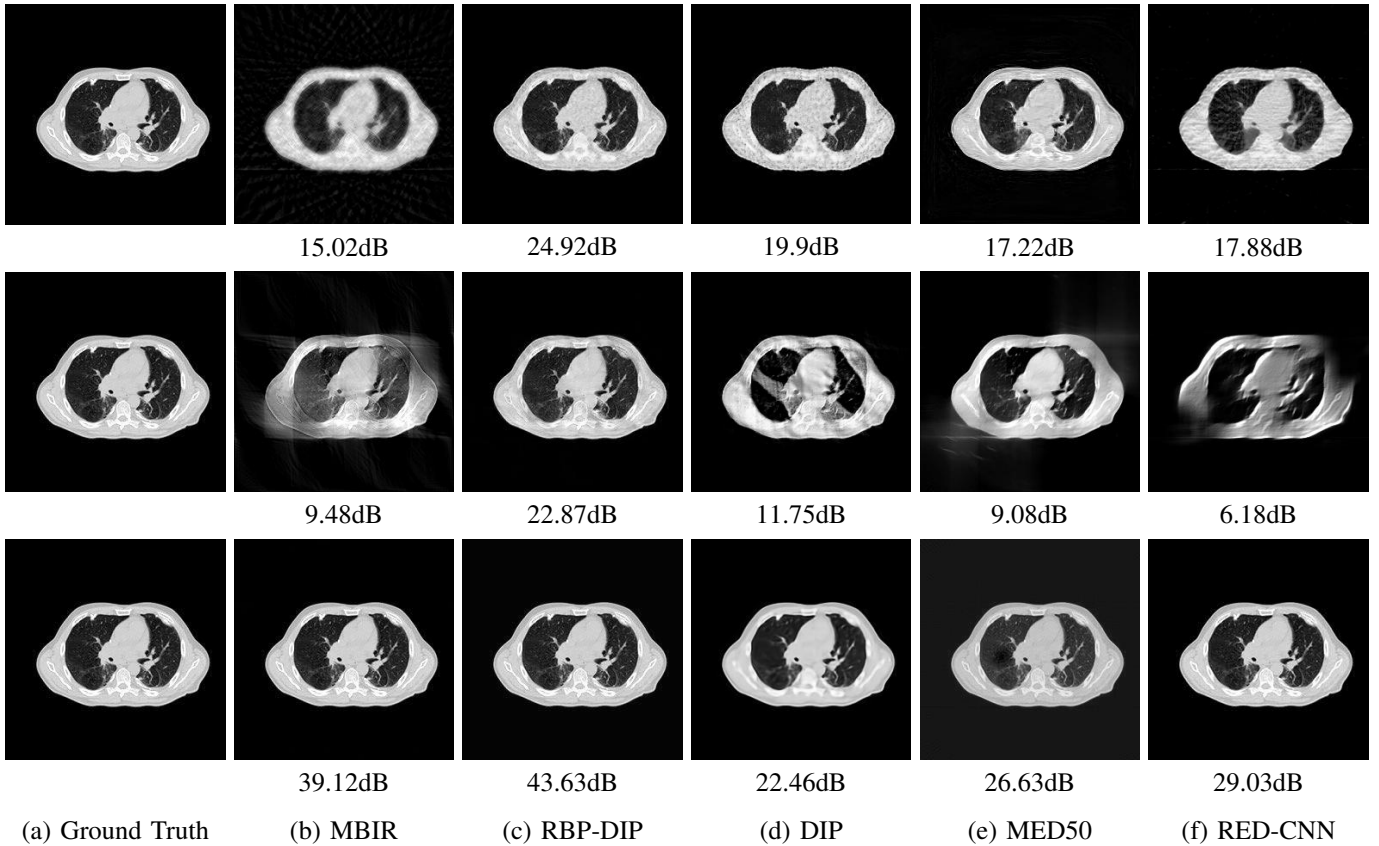


Fig. 2: The reconstructed results of LIDC-IDRI dataset for different methods under sparse-view (first row, 30 projections distributed uniformly from 0° to 180°), limited-angle (second row, 90 projections distributed uniformly from 0° to 90°) and full-view (third row, 180 projections distributed uniformly from 0° to 180°) conditions.

where n indicates the current number of iterations. β is a sigmoid function centered at n_c and stretched by the factor n_s . This extra parameter is used to control the update step size together with α , the original controlling parameter from the steepest descent algorithm. The early stage of reconstruction process ($\frac{n}{n_s} \ll n_c$) is dominated by the U-net structure. In this stage, the DIP can help generate a high-quality preliminary reconstruction results, and the strength of the RBP connection is suppressed by β to avoid the artifacts generated by conventional MBIR methods. Later ($\frac{n}{n_s} \gg n_c$), the strength of the RBP connection will be enhanced as β increases to 10^{-3} . In this stage, the RBP connection can further improve the reconstruction without introducing artifacts, since a high-quality preliminary reconstruction has already been generated.

IV. EXPERIMENTS AND RESULTS

In this section, we will compare our method with the state-of-the-art untrained DIP model [34] and the well-known pre-trained model MED50 [36]. The similarities of the three models' structures show the advantages of the proposed method without model complexity bias. Comparisons with the state-of-the-art pre-trained model RED-CNN [5] are also made, verifying the effectiveness of patch based learning for CT reconstruction. The MBIR method [13] with the steepest descent algorithm [37] is used as a baseline. Due to the

Algorithm 1 RBP-DIP

Input: measure matrix \mathbf{A} , measurement \mathbf{g} , output \mathbf{c} (zero at the beginning), input \mathbf{z} (zero at the beginning), and step size β . The untrained model G indicates the U-net in Fig.4 without the skip connection and the RBP connection.

- 1: $\mathbf{r} = \mathbf{A}^T \mathbf{g} - \mathbf{A}^T \mathbf{A} \mathbf{c}$
 - 2: **Repeat:**
 - 3: $\alpha = \frac{\mathbf{r}^{[:T]T} \mathbf{r}^{[:T]}}{\mathbf{r}^{[:T]T} (\mathbf{A}^T \mathbf{A} \mathbf{r})^{[:T]}}$
 - 4: $\mathbf{z} = \mathbf{c} + \alpha \beta \mathbf{r}$
 - 5: $\mathbf{c} = \mathbf{z} + G(\mathbf{w}; \mathbf{z})$
 - 6: $\mathbf{r} = \mathbf{A}^T \mathbf{g} - \mathbf{A}^T \mathbf{A} \mathbf{c}$
 - 7: update \mathbf{w} by using the Huber loss of \mathbf{r}
 - 8: **Until:** convergence, or some fixed number of iterations is reached.
-

hardware limitation (mainly about training pre-trained models for comparison), the reconstruction resolutions are set to 128×128 and 256×256 . All the mentioned neural networks are implemented in Python with the Pytorch library. The RMSProp algorithm is used for optimization. The learning rate is set to 1×10^{-4} and decreases by a factor of 0.9 per 1000 iterations. Images from LIDC-IDRI [8] (The Lung Image Database Consortium image collection) dataset and COVID-19-NY-SBU [38] (Stony Brook university COVID-19 positive

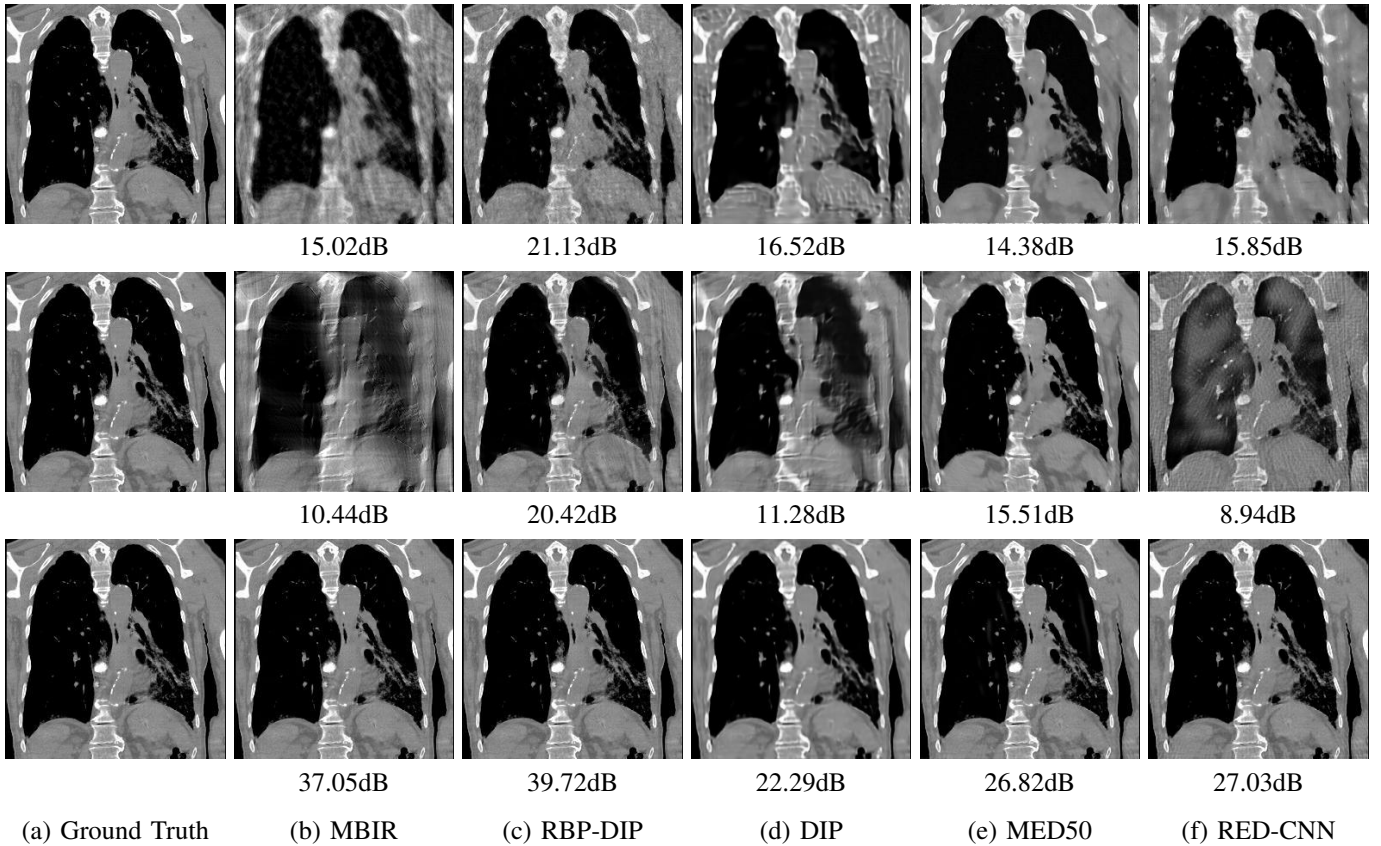


Fig. 3: The reconstructed results of COVID-19-NY-SBU dataset for different methods under sparse-view (first row, 30 projections distributed uniformly from 0° to 180°), limited-angle (second row, 90 projections distributed uniformly from 0° to 90°) and full-view (third row, 180 projections distributed uniformly from 0° to 180°) conditions.

cases) dataset are used in our experiments. However, only the experiment result for LIDC-IDRI is plotted because the latter's result almost exactly follows the trend of LIDC-IDRI.

It is worth mentioning that each pre-trained model is re-trained for different settings such as the number of views, projection angular range, and noise level. Furthermore, test images (but not validation images) are used directly to evaluate the pre-trained models during the training process. Although impractical in the real world, this guarantees that the best reconstruction results of the test images can be obtained.

A. The Effectiveness of RBP Connection

We first show how the newly invented RBP connection helps the neural network reconstruct images better. In Fig.5, the first row shows the reconstruction results for different numbers of iterations; the second row shows the corresponding input updated by the RBP connection, where histogram expansion is performed on all images for better contrast. The number of views is 90, uniformly distributed from 0° to 90° , so it is a limited-angle CT reconstruction problem with high difficulty.

In the first iteration (Fig.5a), the input will be updated by the RBP connection before feeding into the neural network. So this input is just the first iteration output of the steepest descent algorithm multiplied by β . The output is highly randomized since the entire neural network is randomly initialized.

In the 10th iteration (Fig.5b), the deep image prior property helps the model quickly converge to the correct shape, where an object lies in the center and the background is totally black (no streak artifacts caused by the missing projections). The corresponding input image guides the model by highlighting the area requiring correction. In that case, the model will utilize such information more when reconstructing quadrants II and IV, and utilize the deep image prior property more when reconstructing quadrants I and III. As a result, a better reconstruction result is obtained in the 20th iteration (Fig.5c).

In the 2000th iteration (Fig.5d), an acceptable reconstruction result has been generated. At this time, the input mainly focuses on the edges of the object to improve details. Finally, a high-quality reconstruction result can be obtained (Fig.5e). The reconstruction results generated by other methods are shown in the second row of Fig.2, it is evident that the image generated by our proposed method has the highest quality.

A direct comparison between the proposed RBP-DIP method and the current untrained method [34] under the sparse-view condition in terms of reconstruction loss and SNR is shown in Fig.6. The reconstruction loss can be further reduced with the proposed RBP connection, and the reconstruction SNR can be improved by about 8dB, which is significant.

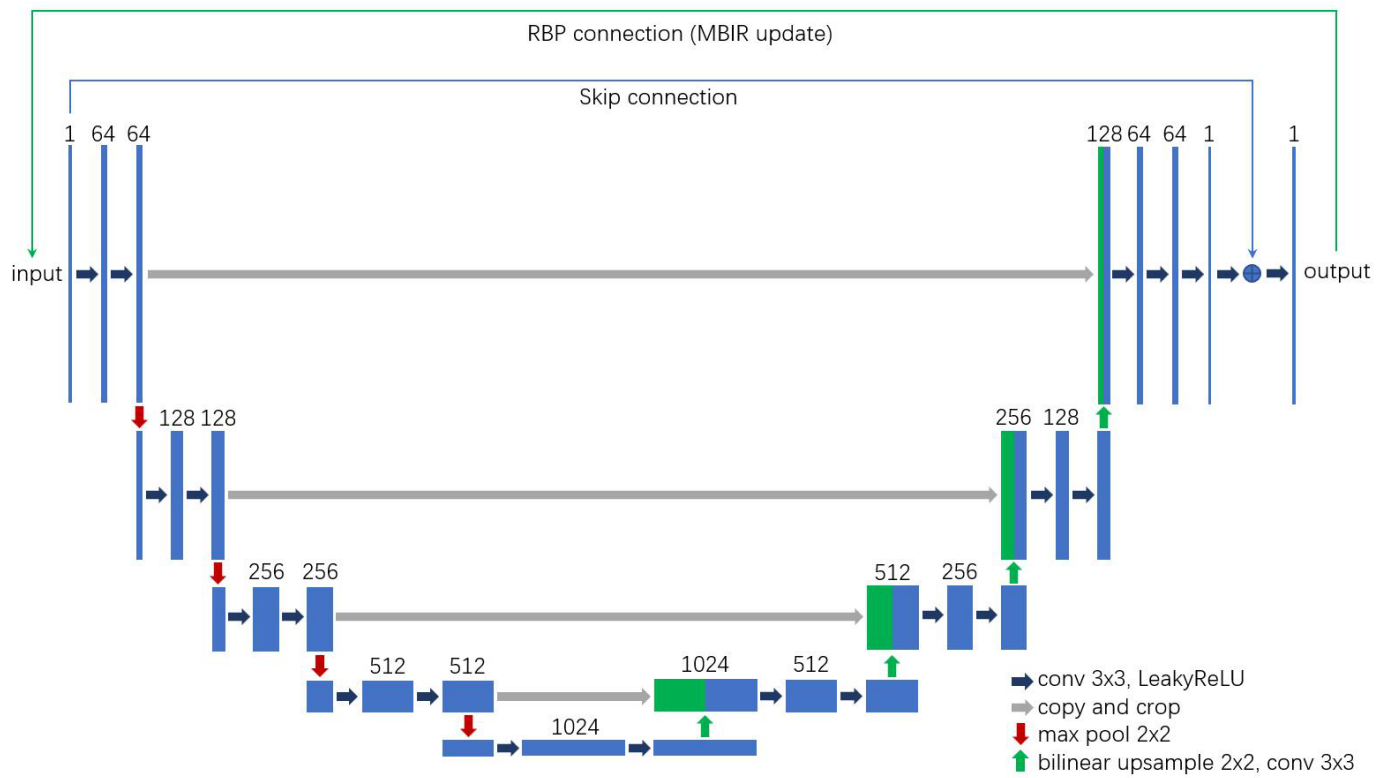


Fig. 4: The architecture of the proposed method, derived from U-net. The skip connection for residual learning and the RBP connection for residual back projection are new and not in the original U-net.

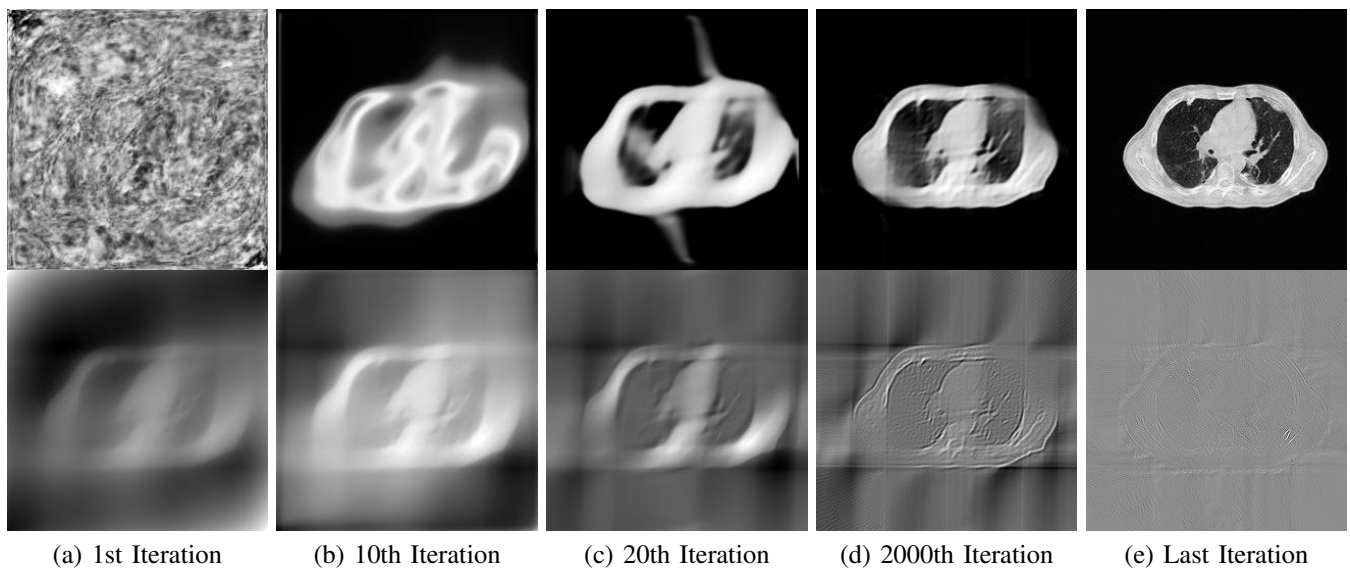
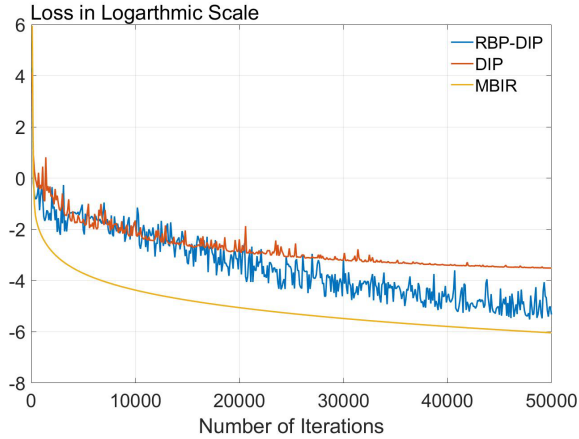
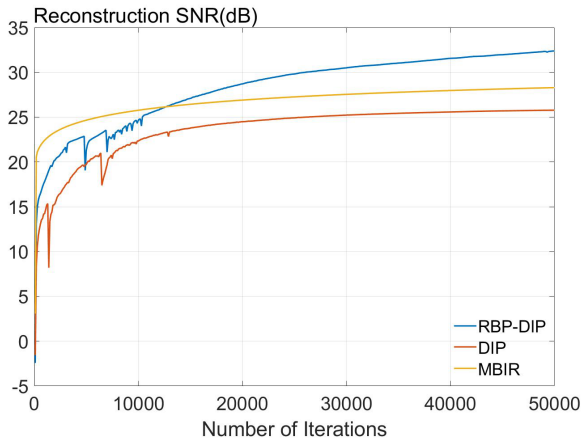


Fig. 5: The output $z + G(w; z)$ (first row) and corresponding input z (second row) at different iteration. The number of views is 90, uniformly distributed from 0° to 90° .



(a)

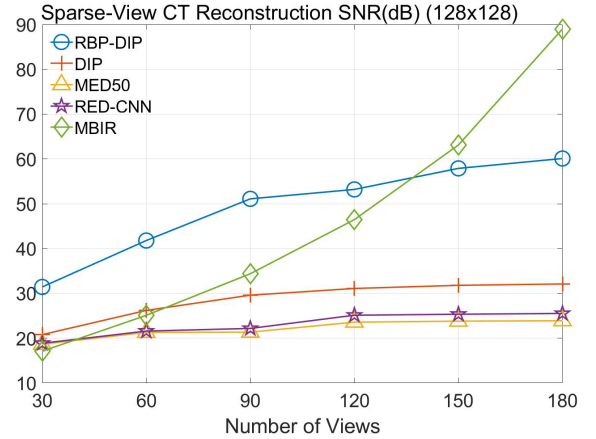


(b)

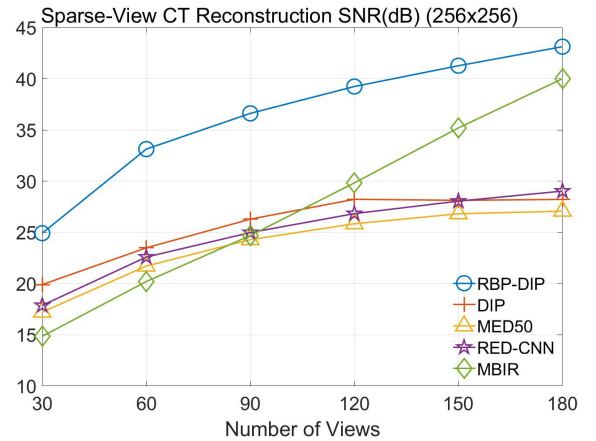
Fig. 6: The reconstruction loss (l_2 norm in logarithmic scale) and SNR (dB) of different methods under sparse-view condition (number of view is 90, uniformly distributed from 0° to 180°). RBP-DIP achieves higher SNR with a loss larger than MBIR method.

B. Sparse-View CT Reconstruction

In this section, the reconstruction performance of our proposed method under sparse-view conditions will be tested. In the experiment, the number of views increases from 30 to 180 and uniformly distributes from 0° to 180° , providing a complete benchmark of reconstruction performance from extremely sparse to complete, full-view CT reconstruction. The same experiment is also done with the aforementioned untrained and pre-trained methods, as well as the MBIR using the steepest descent algorithm. The experiment results are shown in Fig.7. Also, the ground truth, sparse-view (30 views), and full-view (180 views) CT reconstruction results of different methods are shown in the first and third rows of Fig.2 (LIDC-IDRI dataset) and Fig.3 (COVID-19-NY-SBU dataset). It is worth mentioning that the superior performance of MBIR method in Fig.7a is credited to the small number of unknowns. The MBIR method can achieve significantly higher SNR when the number of unknowns is close to or smaller than the number of measurements.



(a)



(b)

Fig. 7: The performance of sparse-view CT reconstruction for different methods under different numbers of views: (a) reconstruction resolution is 128×128 ; (b) reconstruction resolution is 256×256 .

C. Limited-Angle CT Reconstruction

To test the proposed framework's performance on limited-angle reconstruction, we redo the experiment in the above section with the angular range changing from $0^\circ - 90^\circ$ to $0^\circ - 165^\circ$ and one projection per degree. The experiment results are shown in Fig.8. Also, the ground truth and the limited-angle (angular range $0^\circ - 90^\circ$) CT reconstruction results of different methods are shown in the second row of Fig.2 (LIDC-IDRI dataset) and Fig.3 (COVID-19-NY-SBU dataset).

D. Perturbation and Noise

As previously mentioned, one of the most significant advantages of our proposed method is that no training process is required. This advantage eliminates any interference from an inadequate training process or the inconsistencies between inference input and training data. To prove this claim, we redo the sparse-view CT reconstruction experiment with the same test image rotated by 30° degrees, modeling a simple pose change of the patient. The reconstruction performances are

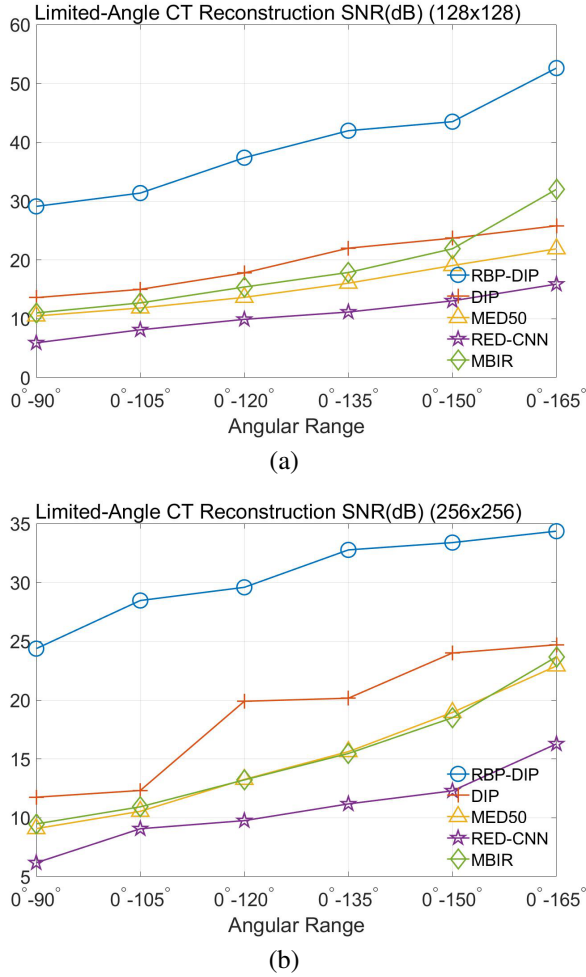


Fig. 8: The performance of limited-angle CT reconstruction for different methods under different angular ranges: (a) reconstruction resolution is 128×128 ; (b) reconstruction resolution is 256×256 .

shown in Fig.9, and the reconstruction results corresponding to 30 views are shown in Fig.10. The comparison is also made under the limited-angle condition, and similar results are obtained.

To test the proposed method's performance under the low-dose condition, we repeat the aforementioned reconstruction experiments by using the sinogram data polluted with Poisson distributed noise. The average number of X-ray photons received by the i th detector can be expressed as:

$$E_i = I_0 e^{[\mathcal{P}\{f\}]_i},$$

where $I_0 > 0$ is the blank measurement ($[\mathcal{P}\{f\}]_i = 0$). It is worth mentioning that the sinogram measurement in our experiment is simulated with the Radon transform instead of obtained from a real instrument. Thus, I_0 here is a parameter for relative measurement. In our experiments, I_0 is set to $10^2, 10^3, \dots, 10^8$, and the corresponding sinogram SNR(dB) is 25.6, 35.6, ..., 85.6. It is worth mentioning that similar experiments are also performed under sparse-view and limited-angle conditions, and the proposed method significantly out-

performs other methods under all conditions. However, such improvement is mainly credited to the superior performance of the proposed method under sparse-measurement conditions rather than better noise resistance performance. For a fair comparison, we only show the results under full view (angular range $0^\circ - 180^\circ$, one view per degree) in Fig.11.

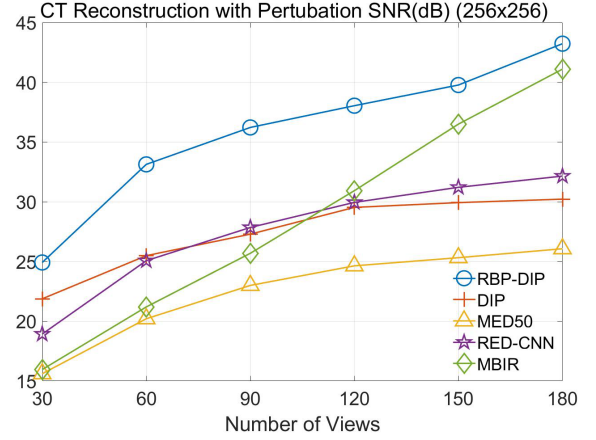


Fig. 9: The performance of sparse-view CT reconstruction with perturbation (rotated by 30°) for different methods.

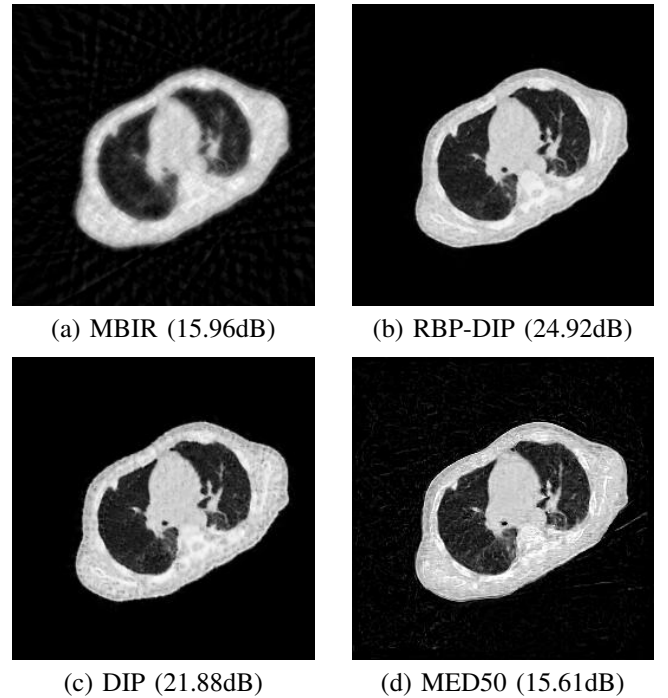


Fig. 10: The sparse-view (30 views) CT reconstruction results with perturbation (rotate by 30°) of different methods.

V. DISCUSSION

A. DIP, MBIR, and RBP Connection

Both the RBP-DIP method and the original DIP method in [34] utilize the deep image prior. The superior performance of the two methods under the sparse-view (Fig.7b, fewer than

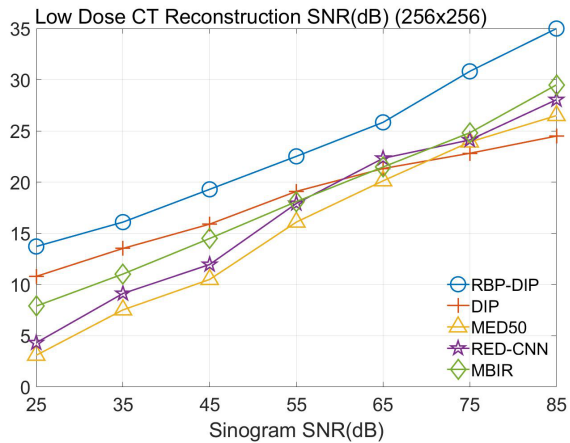


Fig. 11: Effect of quantum noise modeled by Poisson distribution in the sinogram on reconstruction SNR (dB).

120 views) and limited-angle (Fig.8) conditions indicate that such prior is powerful in CT reconstruction. Similar results are also shown in Fig.2c, Fig.2d, Fig.3c, and Fig.3d. The second row of Fig.2d and Fig.3d have very clear boundaries and SNRs higher than those of the MBIR method, despite having neural network specific artifacts. However, the DIP method has its own deficiencies, one being that it cannot easily generate detailed images. As a result, the original DIP model cannot effectively improve its accuracy as the number of measurements increases. For example, in Fig.7b, the MBIR algorithm gets 25dB SNR gain as the number of views increases from 30 to 180, while the DIP method gets only 8dB. The same phenomenon is also shown in Fig.7a and Fig.8. Furthermore, an untrained model may generate images with neural network specific artifacts. This is shown in Fig.12, where an incorrect structure is generated in the early stage (Fig.12a) and hasn't been corrected even after the last iteration (Fig.12b).

MBIR methods are designed to solve (3). An accurate reconstruction result can be obtained when enough measurement is available (Fig.7a, 180 views). Under this condition, the regularizer R sacrifices data fidelity ($\|g - Ac\|^2$) for image regularity. However, the data fidelity term can be minimized by multiple images under the sparse-measurement condition. In that case, regularizers need to not only perform image regularization but also act as a prior, selecting the most reasonable image. It is evident that conventional regularizers cannot fulfill this role, especially when the measurement is too sparse. However, the streak artifacts generated by MBIR can be relatively easily removed by neural network related methods, and an image with meaningful information (second row of Fig.2b) can still be generated.

On the one hand, deep image prior is most effective under the sparse-measurement conditions. However, it cannot help neural networks generate detailed images even when the number of measurements is large enough. On the other hand, conventional MBIR methods cannot generate high-quality reconstruction results under the sparse-measurement conditions, but their results still contain meaningful information. The

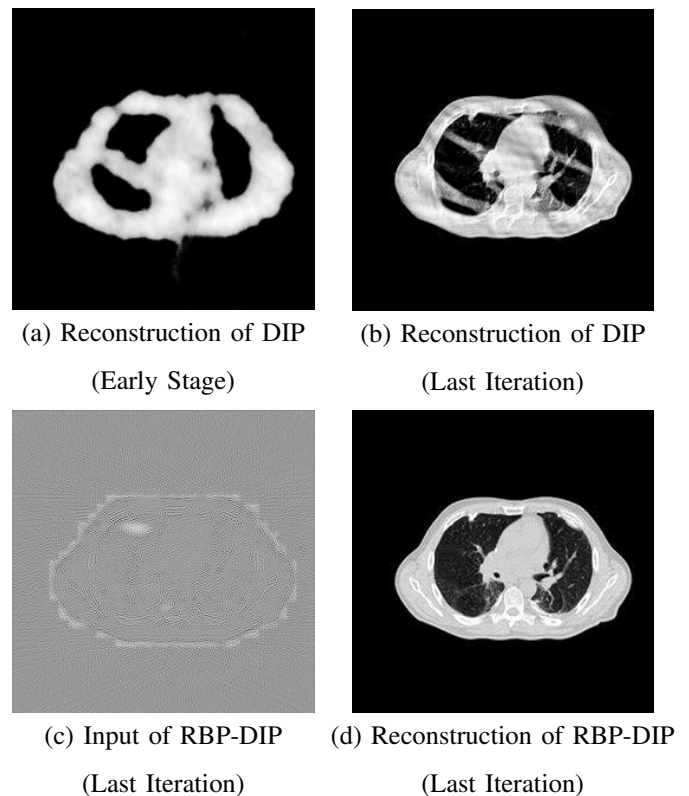


Fig. 12: Reconstruction comparison between DIP and RBP-DIP. DIP algorithm cannot handle the neural network specific artifacts ((a) and (b)), while RBP-DIP can use the RBP connection to guide the model in each iteration ((c) and (d)).

proposed RBP-DIP method combines the two methods using the newly invented RBP connection and possesses advantages from both methods. In Fig.6, the fact that RBP-DIP method achieves an SNR improvement of 5dB over MBIR method despite having a larger loss indicates the effectiveness of deep image prior. Next, the improvement over the original DIP method proves the effectiveness of RBP connection. Furthermore, by using the RBP connection, the neural network specific artifacts shown in Fig.12a and Fig.12b can be corrected effectively. This is because the RBP connection can iteratively update the input image (Fig.12c), and the input image can be used for reconstruction (Fig.12d) indirectly by feeding into the neural network and directly by the skip connection (Fig.5). As a result, significant improvements can be verified in Fig.2, Fig.3, Fig.7, and Fig.8.

B. Comparing with Pre-Trained Model

We have also made comparisons with pre-trained models MED50 and RED-CNN under different conditions. These two models share similar network structures and complexities with the proposed method. We do not choose other models with complicated networks because the proposed method is an untrained method, and a fair comparison should focus on the structural properties of the networks. In Fig.7 and Fig.8, the proposed method outperforms the pre-trained models significantly. Other than the aforementioned advantages of RBP-

DIP, the lack of high-quality training data also degrades the performance of pre-trained models. Comparing to ImageNets, LIDC-IDRI and COVID-19-NY-SBU datasets are not sufficiently large to train a high-performance image reconstruction algorithm. Furthermore, noise- and artifacts-free reconstruction is theoretically unachievable in the scenario of pre-trained neural network methods. This is because the CT images used as ground truth also contain noise and artifacts (generally, CT images with higher doses and more views are used as ground truth). We also find that the RED-CNN outperforms MED50 under sparse-view conditions, but MED50 is better under limited-angle conditions. The reason is that the patch extraction technique used by RED-CNN cannot handle streak artifacts effectively.

Furthermore, Fig.7 and Fig.8 also show that increasing the number of views does not effectively improve the performance of pre-trained models. The reason is that pre-trained models only learn the correlation between the input and output, but not the rule of artifact removal. Increasing the number of views cannot directly enhance the correlation. On the other hand, the proposed RBP-DIP algorithm minimizes the inconsistency between the ground truth and reconstruction images under the same measurement. Increasing the number of views benefits both the network optimization and the MBIR algorithms implemented in the RBP connection. This result is also shown in Fig.2 and Fig.3, where the full-view CT reconstruction result of RBP-DIP is even better than that of MBIR algorithm.

C. Perturbation and Noise

In practice, the imaged object may be inconsistent with the training dataset due to non-ideal factors. The 30° rotation in Section IV-D is a simplified modeling of such inconsistency caused by different poses, and the reconstruction accuracy is shown in Fig.9. Comparing with Fig.7b, it is evident that only the pre-trained method MED50 suffers from a significant SNR drop. Similar results are also shown in Fig.10. Comparing with the first row of Fig.2, the reconstruction result of MED50 does not have an entirely black background and suffers from horizontal artifacts in the non-zero area. This implies that MED50 generates the reconstruction result directly from similar training instances, instead of learning the way of removing artifacts. Thus, it requires a high-quality training dataset and needs to be free of any perturbations. We also redo the experiments under low-dose conditions. As shown in Fig.11, the MED50 is the most vulnerable to sinogram noise. RED-CNN is relatively insensitive to the perturbation because of the patch-based learning technique.

On the other hand, our proposed method does not require any training images and achieves the highest reconstruction accuracy in both experiments. Furthermore, extra constraints can be implemented directly in the loss function or indirectly in the RBP connection to better handle different factors without retraining.

D. Versatility

In this paper, for simplicity and fairness, only the 2D CT reconstruction in parallel-beam geometry is discussed.

The reason to look into parallel-beam geometry is that the forward and back projection can be calculated exactly and efficiently under the parallel-beam geometry [13], [39], so a fair comparison can be made among different methods independent of the error caused by the forward and back projection. Also, the reconstruction resolution does not exceed 256×256 . Should we increase the resolution, the calculation of matrix \mathbf{A} in (1) and the training of the pre-trained models cannot be performed efficiently. However, it is evident that the proposed method can be used for multiple scenarios as the U-net structure is widely used in 2D and 3D images, and the back projection operations in different geometries (corresponding to the RBP connection) are also well analyzed.

The proposed method also has the potential to replace U-nets in other composite models such as [24], [26] or be implemented in other network structures such as U-net++ [40] and ResUnet [41]. The proposed method is compatible with all constraints used in both IR methods and neural network related methods as the constraints can be implemented in the loss function and the RBP connection. Furthermore, unlike other pre-trained models, these constraints can be modified on demand (e.g. increasing the weight of total variation constraint when the input is noisy).

VI. CONCLUSION

In the case of sparse-measurement conditions, IR related methods suffer from streak artifacts, while pre-trained neural network related methods are brittle due to the lack of theoretical guarantee and high-quality training datasets. In this paper, we introduce a new neural network related framework RBP-DIP for X-ray CT reconstruction. It is shown that impressive reconstruction results can be achieved without any training by using RBP-DIP, especially under the sparse-measurement conditions. Such improvements mainly credit to two implementations. The first is the newly invented RBP connection that utilizes the advantages of conventional IR algorithms. The second is the use of the deep image prior. We also show that the proposed method has impressive noise and perturbation resistance performance.

Since the proposed method does not require any training, a fair comparison should be made with conventional IR methods and the original DIP method using a U-net [34]. Comparing with the conventional IR methods, the RBP-DIP can achieve higher SNR even under full-view conditions. Comparing with the original DIP method, the RBP-DIP has better accuracy and benefits more from the increase in the number of views. All these facts imply that our proposed method is a successful implementation that combines the advantages of IR methods and DIP methods.

A complete comparison is also made with pre-trained models sharing similar network structures to RBP-DIP. The impressive improvements prove the excellence of RBP-DIP again. The experiments on the perturbed data show that a pre-trained network is biased toward training data. Such a problem is even more severe in the medical domain, as deviation from normal is the key to diagnosis. In contrast, our untrained RBP-DIP only leverages hierarchical properties of the convolutional

neural network without leveraging what the training data considers normal.

Also, the proposed method is versatile. Unlike pre-trained methods that need to be retrained for different settings and cannot be further adjusted after training, RBP-DIP is compatible with all settings. Extra priors can be implemented on demand in both the RBP connection and the loss function. Furthermore, since the RBP-DIP is designed based on the U-net, which is widely used in multiple neural network related methods and tasks, it can be used in place of U-net or U-net-like networks under multiple conditions.

With these statements, we conclude that the proposed framework is a better choice for solving sparse-view, limited-angle, and low-dose CT reconstruction problems.

DECLARATION OF COMPETING INTEREST

The authors declare that they have no known competing financial interests or personal relationships that could have appeared to influence the work reported in this paper.

REFERENCES

- [1] B. Zhu, J. Z. Liu, S. F. Cauley, B. R. Rosen, and M. S. Rosen, "Image reconstruction by domain-transform manifold learning," *Nature*, vol. 555, no. 7697, pp. 487–492, 2018.
- [2] G. Shen, K. Dwivedi, K. Majima, T. Horikawa, and Y. Kamitani, "End-to-end deep image reconstruction from human brain activity," *Frontiers in Computational Neuroscience*, vol. 13, p. 21, 2019.
- [3] S. Xie, H. Xu, and H. Li, "Artifact removal using gan network for limited-angle ct reconstruction," in *2019 Ninth International Conference on Image Processing Theory, Tools and Applications (IPTA)*. IEEE, 2019, pp. 1–4.
- [4] H. Zhang, L. Li, K. Qiao, L. Wang, B. Yan, L. Li, and G. Hu, "Image prediction for limited-angle tomography via deep learning with convolutional neural network," 2016.
- [5] H. Chen, Y. Zhang, W. Zhang, P. Liao, K. Li, J. Zhou, and G. Wang, "Low-dose ct denoising with convolutional neural network," in *2017 IEEE 14th International Symposium on Biomedical Imaging (ISBI 2017)*. IEEE, 2017, pp. 143–146.
- [6] V. Antun, F. Renka, C. Poon, B. Adcock, and A. C. Hansen, "On instabilities of deep learning in image reconstruction and the potential costs of ai," *Proceedings of the National Academy of Sciences*, vol. 117, no. 48, pp. 30088–30095, 2020.
- [7] J. Deng, W. Dong, R. Socher, L.-J. Li, K. Li, and L. Fei-Fei, "Imagenet: A large-scale hierarchical image database," in *2009 IEEE conference on computer vision and pattern recognition*. Ieee, 2009, pp. 248–255.
- [8] S. G. Armato III, G. McLennan, L. Bidaut, M. F. McNitt-Gray, C. R. Meyer, A. P. Reeves, B. Zhao, D. R. Aberle, C. I. Henschke, E. A. Hoffman et al., "The lung image database consortium (lidc) and image database resource initiative (idri): a completed reference database of lung nodules on ct scans," *Medical physics*, vol. 38, no. 2, pp. 915–931, 2011.
- [9] K. Zhang and A. Entezari, "A convolutional forward and back-projection model for fan-beam geometry," *arXiv preprint arXiv:1907.10526*, 2019.
- [10] B. De Man and S. Basu, "Distance-driven projection and backprojection in three dimensions," *Physics in Medicine & Biology*, vol. 49, no. 11, p. 2463, 2004.
- [11] S. Ha and K. Mueller, "A look-up table-based ray integration framework for 2-d/3-d forward and back projection in x-ray ct," *IEEE transactions on medical imaging*, vol. 37, no. 2, pp. 361–371, 2017.
- [12] Y. Long, J. A. Fessler, and J. M. Balter, "3d forward and back-projection for x-ray ct using separable footprints," *IEEE transactions on medical imaging*, vol. 29, no. 11, pp. 1839–1850, 2010.
- [13] Z. Shu and A. Entezari, "Exact gram filtering and efficient backprojection for iterative ct reconstruction," *Medical Physics*, vol. 49, no. 5, pp. 3080–3092, 2022.
- [14] E. Y. Sidky, C.-M. Kao, and X. Pan, "Accurate image reconstruction from few-views and limited-angle data in divergent-beam ct," *Journal of X-ray Science and Technology*, vol. 14, no. 2, pp. 119–139, 2006.
- [15] X. Jin, L. Li, Z. Chen, L. Zhang, and Y. Xing, "Anisotropic total variation for limited-angle ct reconstruction," in *IEEE Nuclear Science Symposium & Medical Imaging Conference*. IEEE, 2010, pp. 2232–2238.
- [16] T. Wang, K. Nakamoto, H. Zhang, and H. Liu, "Reweighted anisotropic total variation minimization for limited-angle ct reconstruction," *IEEE Transactions on Nuclear Science*, vol. 64, no. 10, pp. 2742–2760, 2017.
- [17] C. Gong and L. Zeng, "Self-guided limited-angle computed tomography reconstruction based on anisotropic relative total variation," *IEEE Access*, vol. 8, pp. 70465–70476, 2020.
- [18] C. Bouman and K. Sauer, "A generalized gaussian image model for edge-preserving map estimation," *IEEE Transactions on image processing*, vol. 2, no. 3, pp. 296–310, 1993.
- [19] R. Zhang, C. A. Bouman, J.-B. Thibault, and K. D. Sauer, "Gaussian mixture markov random field for image denoising and reconstruction," in *2013 IEEE Global Conference on Signal and Information Processing*. IEEE, 2013, pp. 1089–1092.
- [20] S. J. Kisner, E. Haneda, C. A. Bouman, S. Skatter, M. Kourinny, and S. Bedford, "Model-based ct reconstruction from sparse views," in *Second International Conference on Image Formation in X-Ray Computed Tomography*, 2012, pp. 444–447.
- [21] Q. Zhang, J. Gao, Y. Ge, N. Zhang, Y. Yang, X. Liu, H. Zheng, D. Liang, and Z. Hu, "Pet image reconstruction using a cascading back-projection neural network," *IEEE Journal of Selected Topics in Signal Processing*, vol. 14, no. 6, pp. 1100–1111, 2020.
- [22] D. H. Ye, G. T. Buzzard, M. Ruby, and C. A. Bouman, "Deep back projection for sparse-view ct reconstruction," in *2018 IEEE Global Conference on Signal and Information Processing (GlobalSIP)*. IEEE, 2018, pp. 1–5.
- [23] T. Würfl, F. C. Ghesu, V. Christlein, and A. Maier, "Deep learning computed tomography," in *International conference on medical image computing and computer-assisted intervention*. Springer, 2016, pp. 432–440.
- [24] X. Yin, Q. Zhao, J. Liu, W. Yang, J. Yang, G. Quan, Y. Chen, H. Shu, L. Luo, and J.-L. Coatrieux, "Domain progressive 3d residual convolution network to improve low-dose ct imaging," *IEEE transactions on medical imaging*, vol. 38, no. 12, pp. 2903–2913, 2019.
- [25] D. Hu, Y. Zhang, J. Liu, C. Du, J. Zhang, S. Luo, G. Quan, Q. Liu, Y. Chen, and L. Luo, "Special: single-shot projection error correction integrated adversarial learning for limited-angle ct," *IEEE Transactions on Computational Imaging*, vol. 7, pp. 734–746, 2021.
- [26] Y. Zhang, D. Hu, Q. Zhao, G. Quan, J. Liu, Q. Liu, Y. Zhang, G. Coatrieux, Y. Chen, and H. Yu, "Clear: comprehensive learning enabled adversarial reconstruction for subtle structure enhanced low-dose ct imaging," *IEEE Transactions on Medical Imaging*, vol. 40, no. 11, pp. 3089–3101, 2021.
- [27] B. Van Ginneken, A. A. Setio, C. Jacobs, and F. Ciompi, "Off-the-shelf convolutional neural network features for pulmonary nodule detection in computed tomography scans," in *2015 IEEE 12th International symposium on biomedical imaging (ISBI)*. IEEE, 2015, pp. 286–289.
- [28] Y. Bar, I. Diamant, L. Wolf, S. Lieberman, E. Konen, and H. Greenspan, "Chest pathology detection using deep learning with non-medical training," in *2015 IEEE 12th international symposium on biomedical imaging (ISBI)*. IEEE, 2015, pp. 294–297.
- [29] F. Ciompi, B. de Hoop, S. J. van Riel, K. Chung, E. T. Scholten, M. Oudkerk, P. A. de Jong, M. Prokop, and B. van Ginneken, "Automatic classification of pulmonary peri-fissural nodules in computed tomography using an ensemble of 2d views and a convolutional neural network out-of-the-box," *Medical image analysis*, vol. 26, no. 1, pp. 195–202, 2015.
- [30] R. Anirudh, H. Kim, J. J. Thiagarajan, K. A. Mohan, and K. M. Champley, "Improving limited angle ct reconstruction with a robust gan prior," *arXiv preprint arXiv:1910.01634*, 2019.
- [31] Z. Zhang, S. Yu, W. Qin, X. Liang, Y. Xie, and G. Cao, "Self-supervised ct super-resolution with hybrid model," *Computers in Biology and Medicine*, vol. 138, p. 104775, 2021.
- [32] D. Ulyanov, A. Vedaldi, and V. Lempitsky, "Deep image prior," in *Proceedings of the IEEE conference on computer vision and pattern recognition*, 2018, pp. 9446–9454.
- [33] D. V. Veen, A. Jalal, M. Soltanolkotabi, E. Price, S. Vishwanath, and A. G. Dimakis, "Compressed sensing with deep image prior and learned regularization," 2018.
- [34] D. O. Bagger, J. Leuschner, and M. Schmidt, "Computed tomography reconstruction using deep image prior and learned reconstruction methods," *Inverse Problems*, vol. 36, no. 9, p. 094004, 2020.
- [35] Z. Shu and A. Entezari, "Sparse-view and limited-angle ct reconstruction with untrained networks and deep image prior,"

- Computer Methods and Programs in Biomedicine, vol. 226, p. 107167, 2022. [Online]. Available: <https://www.sciencedirect.com/science/article/pii/S016926072200548X>
- [36] K. H. Jin, M. T. McCann, E. Froustey, and M. Unser, "Deep convolutional neural network for inverse problems in imaging," IEEE Transactions on Image Processing, vol. 26, no. 9, pp. 4509–4522, 2017.
- [37] J. R. Shewchuk *et al.*, "An introduction to the conjugate gradient method without the agonizing pain," 1994.
- [38] J. Saltz, M. Saltz, P. Prasanna, R. Moffitt, J. Hajagos, E. Bremer, J. Balsamo, and T. Kurc, "Stony brook university covid-19 positive cases [data set]. the cancer imaging archive."
- [39] Z. Shu and A. Entezari, "Gram filtering and sinogram interpolation for pixel-basis in parallel-beam x-ray ct reconstruction," in 2020 IEEE 17th International Symposium on Biomedical Imaging (ISBI). IEEE, 2020, pp. 624–628.
- [40] Z. Zhou, M. M. Rahman Siddiquee, N. Tajbakhsh, and J. Liang, "Unet++: A nested u-net architecture for medical image segmentation," in Deep learning in medical image analysis and multimodal learning for clinical decision support. Springer, 2018, pp. 3–11.
- [41] Z. Zhang, Q. Liu, and Y. Wang, "Road extraction by deep residual u-net," IEEE Geoscience and Remote Sensing Letters, vol. 15, no. 5, pp. 749–753, 2018.